



## Optimal Path Smoothing with Log-aesthetic Curves Based on Shortest Distance, Minimum Bending Energy or Curvature Variation Energy

R. U. Gobithaasan<sup>1</sup> , S. W. Yip<sup>2</sup> , Kenjiro T. Miura<sup>3</sup>  and S. Madhavan<sup>4</sup> 

<sup>1</sup>University Malaysia Terengganu, [gr@umt.edu.my](mailto:gr@umt.edu.my)

<sup>2</sup>University Malaysia Terengganu, [uriko\\_yip@yahoo.com](mailto:uriko_yip@yahoo.com)

<sup>3</sup>Shizuoka University, [tmiura.kenjiro@shizuoka.ac.jp](mailto:tmiura.kenjiro@shizuoka.ac.jp)

<sup>4</sup>Monash University Malaysia, [madhavan.shanmugavel@monash.edu](mailto:madhavan.shanmugavel@monash.edu)

Corresponding author: R. U. Gobithaasan, [gr@umt.edu.my](mailto:gr@umt.edu.my)

**Abstract.** This paper proposes a novel algorithm to generate an obstacle-avoiding smooth path that optimizes for three types of constraints namely minimum path distance, bending energy or curvature variation energy. In literature, there are various proposals to generate smooth path using typical curves such as Bézier and clothoid. However, complicated curvature computation of Bézier and limited solution provided by clothoid are some of the drawbacks to this problem. The paper proposes Log-Aesthetic Curves (LAC) for path smoothing; the generated smooth paths of our method are made up of bi-LACs, i.e. curves whose curvature is either monotone increase or decrease. This paper also presents few examples of joining given circles and lines with LACs to show its flexibility in providing curvature continuous solutions. Numerous simulations are demonstrated to highlight the superiority of LAC path smoothing technique.

**Keywords:** Log-aesthetic curves, curvature continuity, obstacle-avoiding, path smoothing, minimal arc length, minimum bending energy, minimum variation energy.

**DOI:** <https://doi.org/10.14733/cadaps.2020.639-658>

### 1 INTRODUCTION

Path planning is a process of constructing a desired movement from an initial location into discrete motions which satisfy given constraints before reaching to the final position. In practice, there are two formulation commonly used in path planning; parametric representation such as Bézier or nonlinear representation such as clothoid that generated with Fresnel Integral. Despite cubic Bézier or B-spline has been widely used in CAD/CAM practices, it imposes several unwanted characteristics, e.g. local curvature extrema and complicated curvature or arc length computation. However, natural spirals do not have these problems except for the generation of spiral itself

which involves integration. With the advancement of computer technology nowadays, numerical integration can be carried out with minimal effort while preserving high precision. Runge-Kutta method can be used to generate spirals which greatly reduce computation cost [3]. There are also attempts to represent spirals by means of Bézier [14], however these curves lose their degree of freedom while satisfying curvature monotonicity to mimic spiral.

Typical curves that are commonly used to replace polyline path include Dubins path; the combination of line segments and circular arcs. It is one of the most popular choices in path smoothing [1], but it satisfies only  $G^1$  continuity. Highway design and railway route design has somewhat similar design procedure as compared to path planning. The underlying property is to satisfy given  $G^2$  data which comprises of position, tangent and curvature at the endpoints. Hickerson [7] stated that highway design must avoid sudden changes between curves with different curvatures. He proposed using gradual increase or decrease types of curvature which is in fact the main feature of spirals. Baass [2] has simplified  $G^2$  highways design into five cases using clothoid; (i) line to circle with a single spiral, (ii) circle to circle with a single spiral, (iii) circle to circle forming S-curve with a pair of spirals, (iv) circle to circle forming C-curve with a pair of spirals, and (v) line to line with a pair of spirals. Figure 1 shows the simple illustration of these five cases.

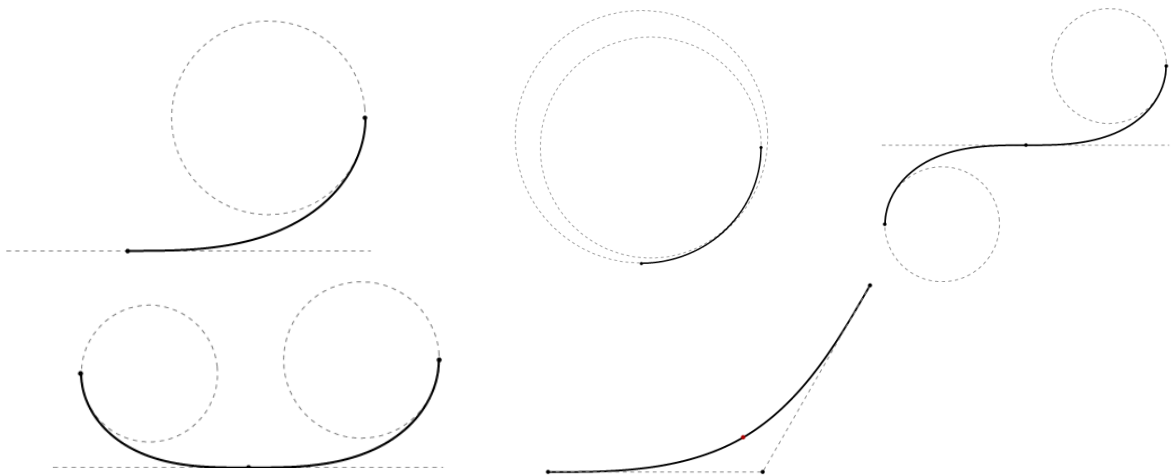


**Figure 1:** A simple illustration of the five cases of clothoid templates that was identified by Baass [2].

There have been many attempts to solve these cases using various types of curves such as Bézier spiral and Pythagorean Hodograph spirals. However, the  $G^2$  solutions are either limited or no feasible solution exist since the proposed method is curve centric. Hence, designers have no option on finding optimum path which minimizes path length, bending energy or curvature variation energy.

Assume numerous obstacles exist in a given planar region and a mobile robot represented as a point has to traverse along a path avoiding those obstacles. It is rather straightforward to draw a guiding polyline path avoiding obstacles to reach to the final destination. The polyline path is then replaced with smooth curves; a process known as path smoothing [9]. Hence, the solution of the fifth case stated by Baass comes in handy where we construct  $G^2$  curves from given polylines.

In this paper, we propose Log-aesthetic Curves (LACs) as an alternative for path smoothing due to its monotonic curvature property, hence free from local curvature extrema [10]. According to Levien and Séquin [8], LAC is a promising curve for industrial and CAD applications due to its

self-affinity property. This elegant feature has made it attractive for applications in various aesthetic related fields such as automobile design [12], shape completion in archeology [4] and architecture design [13].

Let  $S$  be a LAC space representing spirals with 3 shape variables,  $\alpha, c_1, c_2$  [5, 11]. Various family of spirals can be generated by giving specific  $\alpha$  values,  $S = \{s_\alpha \mid \alpha \in R\}$ . A collection of natural spirals  $s_N \subset S$  is obtained when  $\alpha = \{-1, 0, 1, 2\}$  where the spiral families are {clothoid, Neilsen's spiral, Logarithmic spiral, circle involute}. The rest two free variables can be utilized for satisfying design constraints. In 2006, an algorithm to fit LACs to a set of  $G^1$  Hermite data was proposed in [16]. Later, Miura et al. developed an algorithm to implement tri-LACs to solve  $G^2$  Hermite interpolation problem [12].

The following part of this paper is organized as follows. Section 2 introduces the fundamental equations of a single and bi-LAC segments to solve five cases stated by Baass [2]. It is evident that LACs are capable to provide multiple solutions as compared to clothoid as shown in Section 3. Section 4 proposes a four-step algorithm on constructing an obstacle-avoiding path that are optimized based on three types of constraints; shortest distance, minimum bending energy or minimum curvature variation energy. Numerous simulation results are presented in Section 5 to show the validity of the proposed algorithm. Finally, we conclude this paper with a plan of future works in Section 6.

## 2 ANALYTICAL FORMULAS AND PARAMETERS

This section presents the important equations of a single and bi-LACs segment. The equations are intrinsically simple and the derivation will be based on the fundamental equation that was coined by Miura [10]. For the sake of simplicity, we assume that the curvature of LACs  $\kappa \geq 0$  and its shape parameter  $\alpha \neq 0, 1$ . (2.1) below is the curvature function  $\kappa(\tilde{s})$  of a single LACs segment:

$$\kappa(\tilde{s}) = \frac{(c_0\tilde{s} + c_1)^{-\frac{1}{\alpha}}}{L}, \quad 0 \leq \tilde{s} \leq 1 \quad (2.1)$$

where  $\tilde{s}$  represents arc length,  $L$  be the total length of curve, and  $c_0, c_1$  are constants.

By using the definition of  $\theta'(\tilde{s}) = \kappa(\tilde{s})$ , one can obtain the tangential angle function of the curve as shown in (2.2).

$$\theta(\tilde{s}) = \frac{\alpha}{(\alpha-1)c_0} (c_0\tilde{s} + c_1)^{\frac{\alpha-1}{\alpha}} + c_2, \quad 0 \leq \tilde{s} \leq 1 \quad (2.2)$$

(2.2) is then used to define parametric expressions for LACs coordinates as shown in (2.3) below.

$$\{x_s(\tilde{s}), y_s(\tilde{s})\} = \left\{ x_0 + L \int_0^{\tilde{s}} \cos \theta(\tilde{s}) d\tilde{s}, y_0 + L \int_0^{\tilde{s}} \sin \theta(\tilde{s}) d\tilde{s} \right\} \quad (2.3)$$

It is notable that the curvature of LACs is either monotonically increasing or decreasing. Therefore, in the case of joining two lines segments where the initial and final curvatures are both 0, we require at least two pieces of LACs segments to ensure a smooth transition between them. The curvature function  $\kappa(\tilde{s})$ , tangent angle  $\theta(\tilde{s})$  and parametric expression of a bi-LACs segment are shown in (2.4), (2.5) and (2.6), respectively.

$$\kappa(\tilde{s}) = \begin{cases} \frac{(c_{10}\tilde{s} + c_{11})^{-\frac{1}{\alpha}}}{L}, & 0 \leq \tilde{s} \leq s \\ \frac{(c_{20}\tilde{s} + c_{21})^{-\frac{1}{\alpha}}}{L}, & s < \tilde{s} \leq 1 \end{cases} \quad (2.4)$$

$$\theta(\tilde{s}) = \begin{cases} \frac{\alpha}{(\alpha-1)c_{10}} (c_{10}\tilde{s} + c_{11})^{\frac{\alpha-1}{\alpha}} + c_{12}, & 0 \leq \tilde{s} \leq s \\ \frac{\alpha}{(\alpha-1)c_{20}} (c_{20}\tilde{s} + c_{21})^{\frac{\alpha-1}{\alpha}} + c_{22}, & s < \tilde{s} \leq 1 \end{cases} \quad (2.5)$$

$$\{x_b(\bar{s}), y_b(\bar{s})\} = \left\{ x_0 + L \left( \int_0^s \cos \theta(\bar{s}) d\bar{s} + \int_s^1 \cos \theta(\bar{s}) d\bar{s} \right), y_0 + L \left( \int_0^s \sin \theta(\bar{s}) d\bar{s} + \int_s^1 \sin \theta(\bar{s}) d\bar{s} \right) \right\} \quad (2.6)$$

A curve is  $G^2$  continuous if and only if it satisfies given positional, tangent as well as curvature at the endpoints. Bi-LAC is introduced in this paper so that we have enough shape parameters to satisfy  $G^2$  conditions. The following part introduces the conditions at the endpoints of a bi-LAC segments once we substitute different  $\bar{s}$  values to (2.4), (2.5) and (2.6).

- When  $\bar{s} = 0$ :

$$\kappa_0 = \frac{(c_{11})^{-\frac{1}{\alpha}}}{L} \quad (2.7)$$

$$\theta_0 = \frac{\alpha}{(\alpha-1)c_{10}} (c_{11})^{\frac{\alpha-1}{\alpha}} + c_{12} \quad (2.8)$$

- When  $\bar{s} = s$ :

$$(c_{10}s + c_{11}) = (c_{20}s + c_{21}) \quad (2.9)$$

$$\frac{\alpha}{(\alpha-1)c_{10}} (c_{10}s + c_{11})^{\frac{\alpha-1}{\alpha}} + c_{12} = \frac{\alpha}{(\alpha-1)c_{20}} (c_{20}s + c_{21})^{\frac{\alpha-1}{\alpha}} + c_{22} \quad (2.10)$$

- When  $\bar{s} = 1$ :

$$\kappa_1 = \frac{(c_{20}+c_{21})^{-\frac{1}{\alpha}}}{L} \quad (2.11)$$

$$\theta_1 = \frac{\alpha}{(\alpha-1)c_{20}} (c_{21})^{\frac{\alpha-1}{\alpha}} + c_{22} \quad (2.12)$$

$$X = x_0 + L \left( \int_0^s \cos \theta(\bar{s}) d\bar{s} + \int_s^1 \cos \theta(\bar{s}) d\bar{s} \right) \quad (2.13)$$

$$Y = y_0 + L \left( \int_0^s \sin \theta(\bar{s}) d\bar{s} + \int_s^1 \sin \theta(\bar{s}) d\bar{s} \right) \quad (2.14)$$

The unknowns:  $\{s, L, c_{ij}, \text{ where } i = 1, 2 \text{ and } j = 0, 1, 2\}$  can be determined from (2.7) to (2.14) once we impose the given  $G^2$  Hermite data to the equations above.

### 3 JOINING LACS TO CIRCLES AND LINES

This section shows some numerical examples of joining given circles and lines with a single and bi-LACs segment. Based on the examples, we found that LACs are more flexible in providing curvature continuous solutions. There are five cases of transition taken into consideration [5]:

- Line to circle with a single LACs
- Circle to circle with a single LACs
- Circle to circle forming S-curve with a bi-LACs
- Circle to circle forming C-curve with a bi-LACs
- Line to line with a bi-LACs

The following sections shows the geometric setup of each case and the condition for the existence of a  $G^2$  LACs solution.

#### 3.1 Line to Circle with a Single LACs Segment

**Setting:** Assume that a line is given on the x-axis and the centre of a given circle is located in the first quadrant. Let R be the radius of the circle and the distance of the line to the centre of the circle denoted as T.

**Condition:** Note that the curvature of a line is 0. Therefore, the value of the shape parameter  $\alpha$  in this case must be  $\alpha < 0$ .

- When  $\alpha = -1$ :  
The solution of clothoid can always be obtained when  $T > R$ . The parameter value of T and R in Figure 2(a) is 1.10147 and 0.8, respectively.
- When  $\alpha \rightarrow -\infty$ :

The solution can be obtained when  $T = R$  as LAC tends to become circle when  $\alpha \rightarrow -\infty$ . The parameter value of T and R in Figure 2(b) is 0.8. Figure 3 illustrates the curvature profile of Figure 2(b) where it shows the curvature of LAC changes monotonically. To note, there is no solution could be found when  $T < R$  as it is geometrically improper.

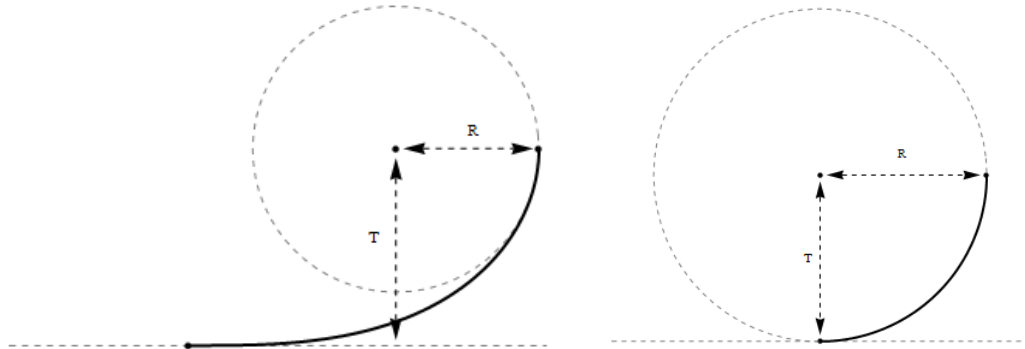


**Figure 2:** Line to circle with a single LACs segment. The black curve is the LACs segment: (a)  $\alpha = -1$ , and (b)  $\alpha = -10000$ .

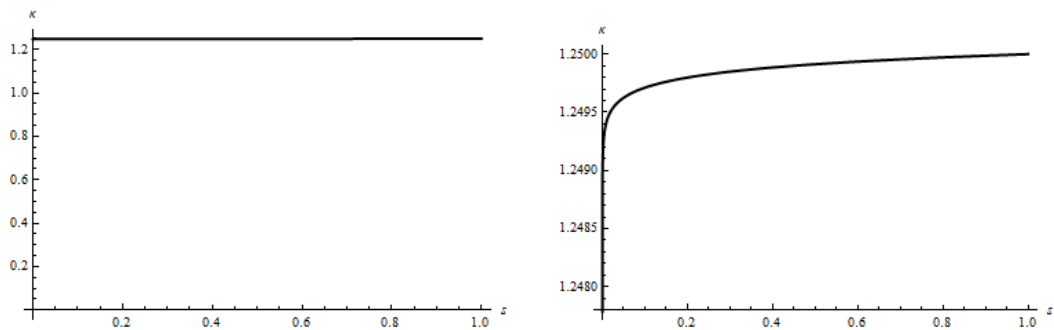


**Figure 3:** The curvature profile of Figure 1(b) in two view versions: (a) General version, and (b) Zoom in version.

### 3.1.1 Dubins path

Dubins path is composed of line segments and circular arcs. The drawback of this approach is that there is a curvature discontinuity at the transition point between circular arc and line. Figure 4(a) shows the CLC type of Dubins path that satisfies only  $G^1$  continuity. In Figure 4(b), we replace the circular arcs with LAC segments and found that it retains the shape as well as length of the original path. Moreover, it provides  $G^2$  continuity at the transition point.

## 3.2 Circle to Circle with a Single LACs Segment

**Setting:** Given two circles such that their corresponding centres are located in the first quadrant and the distance between the centres is denoted as  $D$ . Let the radius of the larger circle be  $R_0$  and the smaller circle be  $R_1$ .

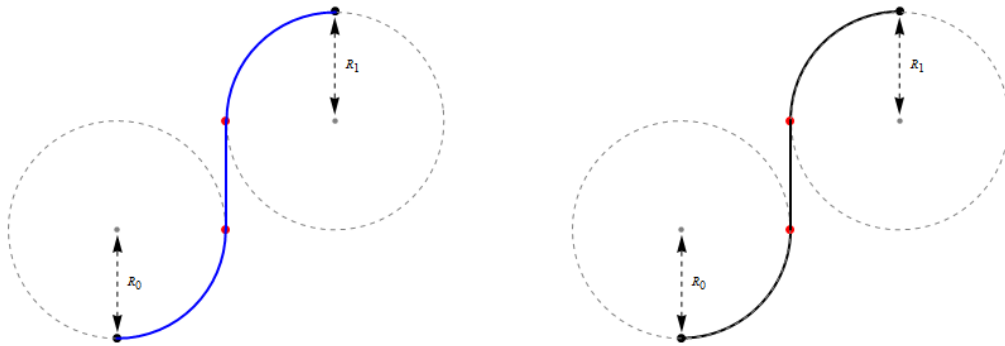


**Figure 4:** The CLC type of transition using two types of curves: (a) Circular arc, and (b) LACs segment.

**Condition:**

- When  $\alpha = -1$ :  
The solution of clothoid can always be obtained when  $R_0 - R_1 > D$ . The parameter value of  $R_0$ ,  $R_1$  and  $D$  in Figure 5(a) is 0.8, 0.7 and 0.09, respectively.
- When  $\alpha \rightarrow \pm\infty$ :  
The solution can be obtained when  $R_0 - R_1 = D$  as LAC tend to mimic circle when  $\alpha \rightarrow \pm\infty$ . The parameter value of  $R_0$ ,  $R_1$  and  $D$  in Figure 5(b) and (c) is 0.8, 0.7 and 0.1, respectively. To note, there is no solution could be found when  $R_0 - R_1 < D$  as it is geometrically improper.

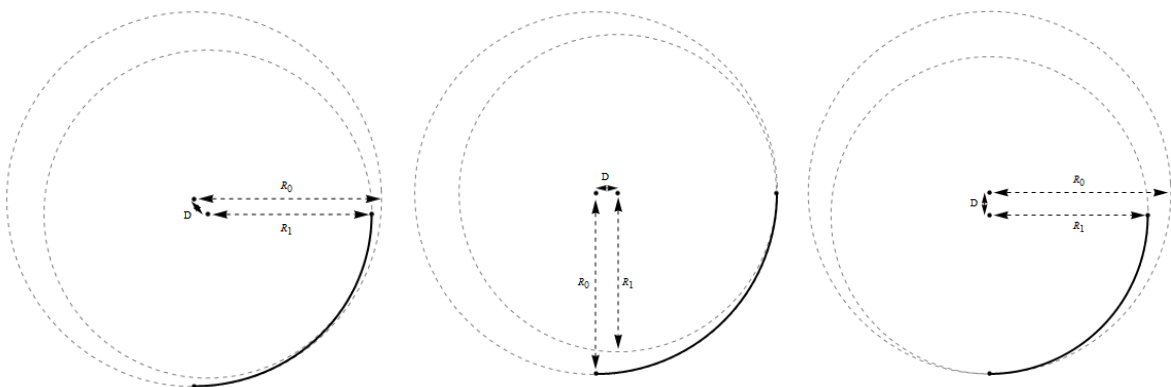


**Figure 5:** Circle to circle with a single LAC segment. The black curve is the LAC segment: (a)  $\alpha = -1$ , (b)  $\alpha = 10000$ , and (c)  $\alpha = -10000$ .

### 3.3 Circle to Circle Forming an S-curve with a bi-LACs Segment

**Setting:** Given two circles of radii  $R_0$  and  $R_1$ . Let the centre of the circle of radius  $R_0$  be located in the third quadrant whereas the centre of the circle of radius  $R_1$  locates in the first quadrant. The parameter  $D$  represents distance between the centres of the circles. Let the curve segments join at the origin where both of its tangent and curvature are equally zero.

**Condition:**

- When  $\alpha = -1$ :  
The solution of clothoid can always be obtained when  $R_0 + R_1 < D$ . The parameter value of  $R_0$ ,  $R_1$  and  $D$  in Figure 6(a) is 0.8, 0.8 and 3.1994, respectively.
- When  $\alpha \rightarrow -\infty$ :  
The solution can be obtained when  $R_0 + R_1 = D$ . The parameter value of  $R_0$ ,  $R_1$  and  $D$  in Figure 6(b) is 0.8, 0.8 and 1.6, respectively. To note, there is no solution could be found when  $R_0 + R_1 > D$  as it is geometrically improper.

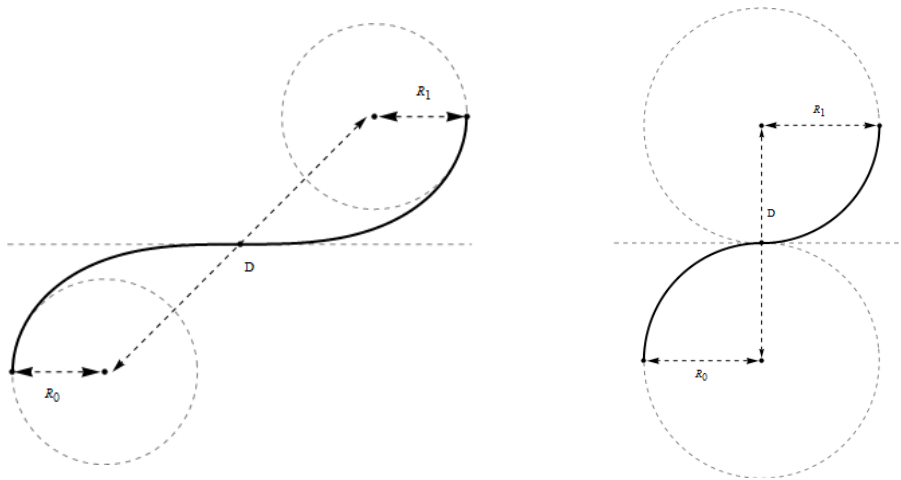


**Figure 6:** Circle to circle forming an S-curve with a bi-LAC segment. The black curve is the LACs segment: (a)  $\alpha = -1, -1$ , and (b)  $\alpha = -10000, -10000$ .

### 3.4 Circle to Circle Forming a C-curve with a bi-LAC Segment

**Setting:** Given two circles of radii  $R_0$  and  $R_1$ . Let the centre of the circle of radius  $R_0$  be located in the second quadrant whereas the centre of the circle of radius  $R_1$  locates in the first quadrant. The parameter  $D$  represents distance between the centres of the circles. Let the curve segments join at the origin where both of its tangent and curvature are equally zero.

**Condition:** As stated below.

- When  $\alpha = -1$ :  
The solution of clothoid can always be obtained when  $|R_0 - R_1| < D$ . The parameter value of  $R_0$ ,  $R_1$  and  $D$  in Figure 7(a) is 0.7, 0.8 and 2.17952, respectively.
- When  $\alpha \rightarrow -\infty$ :  
The solution can be obtained when  $|R_0 - R_1| = D$  as shown in Figure 7(b) and  $|R_0 - R_1| > D$  as presented in Figure 7(c). The parameter value of  $D$  in Figure 7(b) is 0.1 whereas in Figure 7(c), it has value 0.09292. The parameter value of  $R_0$  and  $R_1$  in both figures is 0.7 and 0.8, respectively.

### 3.5 Line to Line with a bi-LACs Segment

**Setting:** Given two lines connected at the end. Without loss of generality, one of the line segments is parallel to the x-axis and another one is located in the positive y-axis region. Let  $d_1$  and  $d_2$  be the length of the corresponding line segments.

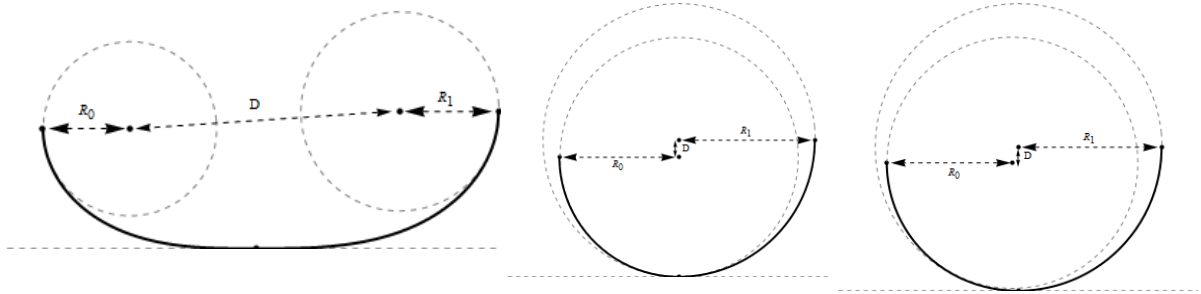


**Figure 7:** Circle to circle forming a C-curve with a bi-LAC segment. The black curve is the LAC segment: (a)  $\alpha = -1, -1$ , (b)  $\alpha = -10000, -10000$ , and (c)  $\alpha = -30, -10000$ .

**Condition:** The solution of clothoid can always be obtained [15]. However, Figure 8 shows that bi-LAC has extra flexibility in providing transition curve with  $G^2$  continuity. The line length for the case below,  $d_1$  and  $d_2$  is 1.

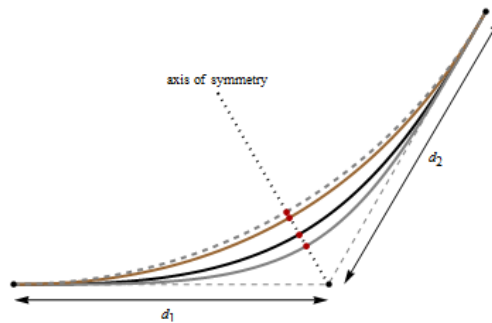


**Figure 8:** Line to line with a bi-LAC segment where  $d_1 = d_2$ . The LACs segment from top to down:  $\alpha = -100, -5, -1$  and  $-1/2$ .

### 3.5.1 Symmetric and asymmetric case

Line to line transitions can be categorized into two cases; symmetric and asymmetric. Figure 9 illustrates the comparison result of a simple example of symmetric and asymmetric case with straight line, circular arc and multiple LAC solutions. Table 1 and Table 2 show the  $\alpha$  value, curve length  $L$ , bending energy  $E$  and curvature variation energy  $V$  of each curve solution. Based on the numerical result, we can deduce the relation of  $\alpha$  and its curve length and energy. This information will be useful to the proposed algorithm below.

## 4 THE PROPOSED ALGORITHM

This section presents an algorithm that generates a smooth obstacle-avoiding path with LACs. Assume that an optimal polyline path is given in a planar region that contains some obstacles. To note, the guiding polyline path can be obtained by using any path planning techniques that is available in literature such as visibility graph or medial axis algorithms. Since LACs provide many feasible paths, an optimal path can be chosen based on three metrics denoted as  $M^*$  below:



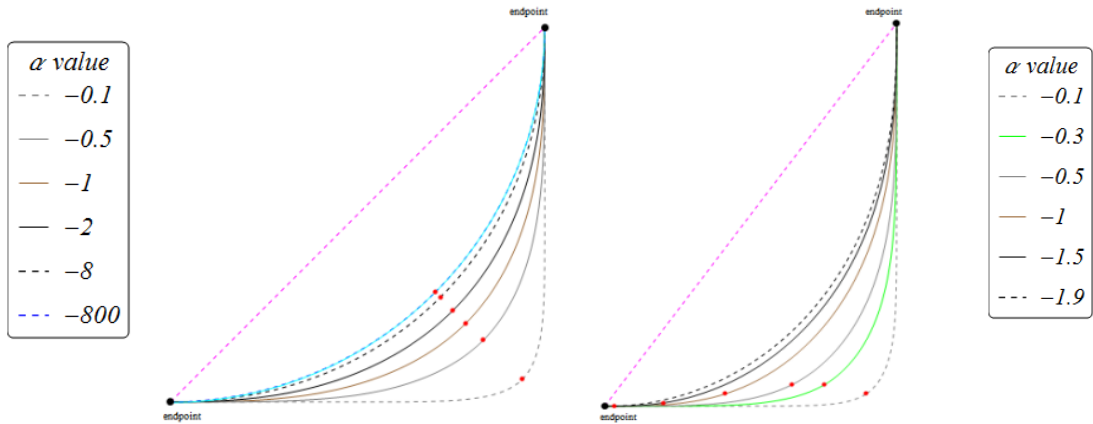


**Figure 9:** A simple line to line transition with straight line (dashed magenta), circular arc (solid cyan) and multiple  $\alpha$  solutions. Two cases are: (a) Symmetric case, and (b) Asymmetric case.

Curve / $\alpha$	$L$	$E$	$V$
Straight line	7.071	0	0
Circular arc	7.854	0.3142	0
-0.1	9.523	1.4929	660
-0.5	8.729	0.5088	13.567
-1	8.399	0.3917	4.7001
-2	8.164	0.34	17.535
-8	7.94	0.3146	616.241
-800	7.854	0.3141	938.373

**Table 1:** The metric values of each solution in Figure 9(a).

Curve / $\alpha$	$L$	$E$	$V$
Straight line	8.602	0	0
-0.1	11.421	1.2448	575.363
-0.3	10.783	0.5604	36.83
-0.5	10.437	0.4255	13.196
-1	10	0.329	5.968
-1.5	9.778	0.3004	10.061
-1.9	9.657	0.29	180.88

**Table 2:** The metric values of each solution in Figure 9(b).

$$M^* = \begin{cases} L, & L: \text{Arc Length} \\ \frac{1}{L} \times \int_0^1 \kappa(\xi)^2 d\xi, & E: \text{Bending Energy} \\ \frac{1}{L} \times \int_0^1 \kappa'(\xi)^2 d\xi, & V: \text{Curvature Variation Energy} \end{cases} \quad (4.1)$$

The shape parameter  $\alpha$  is modified to obtain a curvature continuous collision free path satisfying the chosen metric. The proposed path smoothing algorithm is generally divided into four steps:

- i. Identifying shape of the polyline and partitioning it into C-shaped sections
- ii. Identifying variable values that satisfy  $G^2$  conditions

- iii. Smoothing polyline with default  $\alpha$  (initialization)
- iv. Optimizing shape parameter  $\alpha$  based on chosen metric  $M^*$

Path Smoothing Algorithm below describes the steps of using LACs for generating a collision free path that satisfies given  $G^2$  Hermite data. The flowchart of this algorithm is presented in Figure 10.

### Path Smoothing Algorithm

**Remark:** Polyline path,  $G^2$  Hermite data, initial value of LAC, positive step size and tolerance are given. Let  $M^*$  be the chosen metric by user. An optimal smooth collision free path that satisfies the given  $G^2$  Hermite data is generated and its  $\alpha$  value is identified.

**Input :** Polyline path,  $\{x_0, y_0, X, Y, \theta_0, \theta_1, \kappa_0, \kappa_1\}$ ,  $\alpha_{int}$ ,  $h$  and  $Tol$ .

**Output:** An optimal smooth collision free path satisfying given  $G^2$  Hermite data and its  $\alpha$  value  $\alpha_{opt}$ .

#### Begin

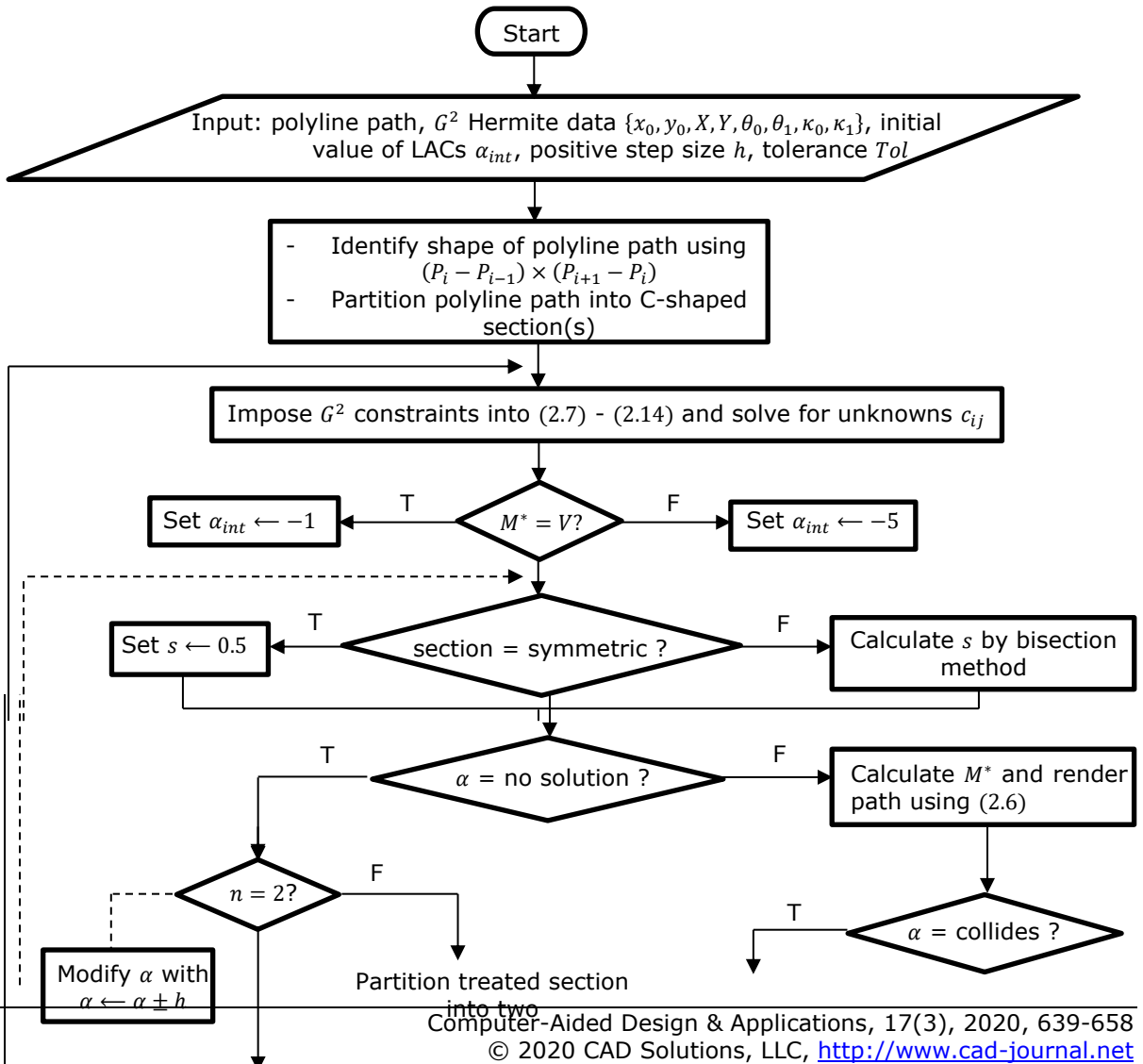
```

Step 1      Identify shape of the given polyline path by using  $(P_i - P_{i-1}) \times (P_{i+1} - P_i)$ .
            Partition polyline path into C-shaped sections (if necessary).
Step 2      Impose  $G^2$  constraints into (2.7) – (2.14) and solve for unknown variables  $c_{ij}$ .
Step 3      Set default  $\alpha \leftarrow \alpha_{int}$ .
            If  $M^* = V$ 
            |   set  $\alpha_{int} \leftarrow -1$ 
            else
            |   set  $\alpha_{int} \leftarrow -5$ 
Step 4      Check:
            If section = symmetric
            |   set  $s \leftarrow 0.5$ 
            else
            |   calculate  $s$  by bisection method
Step 5      Test:
            If  $\alpha = no\ solution$ 
            |   proceed to next step
            Step 6      Check:
            |           If  $n = 2$ 
            |           |   add straight line to polyline path and repeat Step 2-5 or
            |           |   modify  $\alpha$  with  $\alpha \leftarrow \alpha \pm h$  and repeat Step 4-5 (optional)
            |           else
            |           |   further partition polyline path into two and repeat Step 2-5 or
            |           |   modify  $\alpha$  with  $\alpha \leftarrow \alpha \pm h$  and repeat Step 4-5 (optional)
            else
            |   calculate  $M^*$  and render the path using (2.6)
Step 7      Identify path feasibility using collision detection method based on point-region
            intersection.
            If  $\alpha \neq collides$ 
            |   proceed to next step
            else
            |   calculate distance threshold  $\varepsilon$  and shoulder point  $sp$  (collision detection method
            |   based on distance threshold) and proceed to next step
Step 8      Check:
            If  $\alpha \neq collides$  and  $M^* = V$ 
            |
  
```

```

 $\alpha_{opt} \leftarrow \alpha$ ; STOP
else if  $\alpha \neq collides$ 
  do Step 9 and Step 10
  Step 9      Update  $\alpha$  with  $\alpha_{new} \leftarrow \alpha - h$  and repeat Step 4-7
  Step 10    Check:
              If  $\alpha_{new} \neq collides$ 
                do Step 9 and Step 10 until  $\forall M^* < Tol$ 
                 $\alpha_{opt} \leftarrow \alpha_{new}$ ; STOP
              else if  $\alpha_{new} = no\ solution$ 
                reduce  $h \leftarrow h/2$  and repeat Step 9 and Step 10
              else
                 $\alpha_{opt} \leftarrow \alpha$ ; STOP
else
  update  $\alpha$  with  $\alpha_{new} \leftarrow \alpha \pm h$  until  $\forall sp > \epsilon$ 
  repeat Step 10
  
```

End



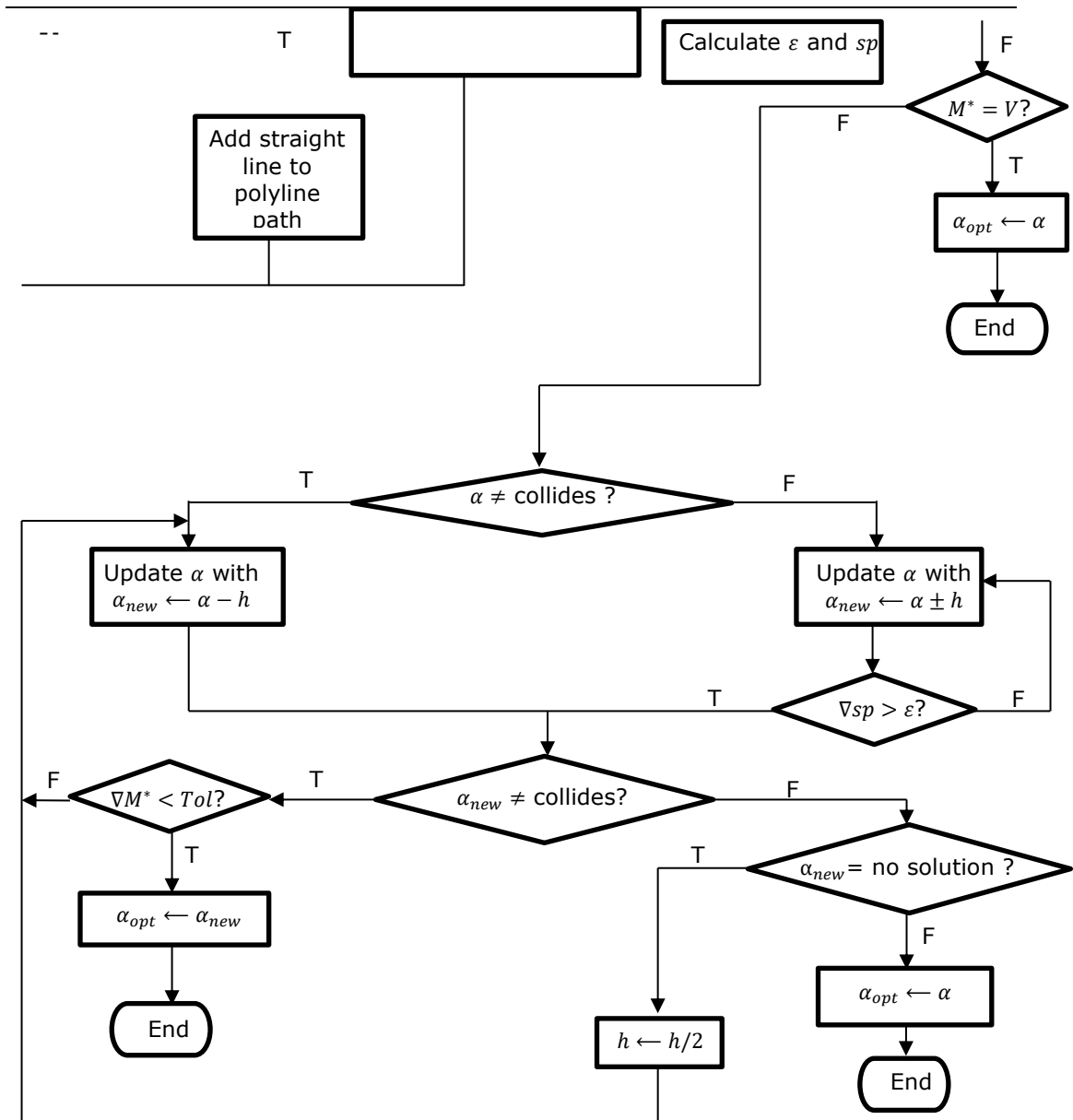


**Figure 10:** The flowchart of the path smoothing algorithm.

#### 4.1 Description of the Path Smoothing Algorithm

The following part gives the detail explanation on each step of the path smoothing algorithm.

##### 4.1.1 Identifying shape of the polyline path and partitioning it into C-shaped sections

A given guiding polyline path is defined to be a C-shape if the cross products of its vertices are all positives or all negatives. The formula of the cross product is shown below:

$$(P_i - P_{i-1}) \times (P_{i+1} - P_i), \quad i = 1, 2, \dots, n - 1 \quad (4.2)$$

Once the shape is identified, we partition the polyline into few C-shaped sections as proposed in [9]. It is noticeable that joining two quadratic Bézier curves with continuous tangent direction at the joint point can form an S-curve. Hence, the partition method treats three adjacent lines at a time. If the three adjacent line segments form an S shape, we will add a new interpolating point to the midpoint of the second line segment. Figure 11 depicts an example of partitioning a polyline path into three C-shaped sections.

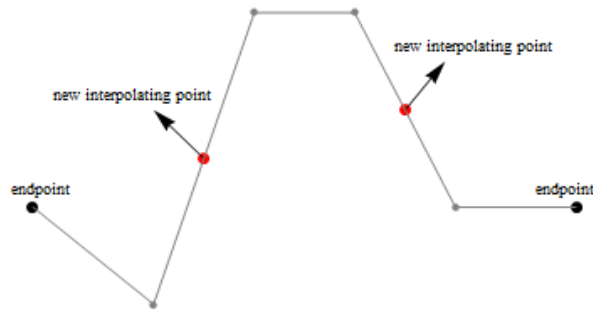


**Figure 11:** Partition the given polyline path into three C-shaped sections.

4.1.2 Identifying variable values that satisfy  $G^2$  conditions

Note that the C-shaped sections after partition process are treated separately. We impose the given  $G^2$  constraints to (2.7) - (2.12) and solve for the unknown variables  $c_{ij}$  where  $i = 1,2$  and  $j = 0,1,2$ . The remaining unknowns  $s$  and  $L$  are determined from (2.13) - (2.14) by bisection method. The parameter  $s$  indicates the arc length of the first segment of a spiral path. Figure 12 and Figure 13 illustrate an example of symmetric and asymmetric C-shaped section with two lines ( $n = 2$ ). For symmetric cases, we set the value of  $s = 0.5$ ; while in asymmetric cases, we may calculate  $s$  using bisection method.

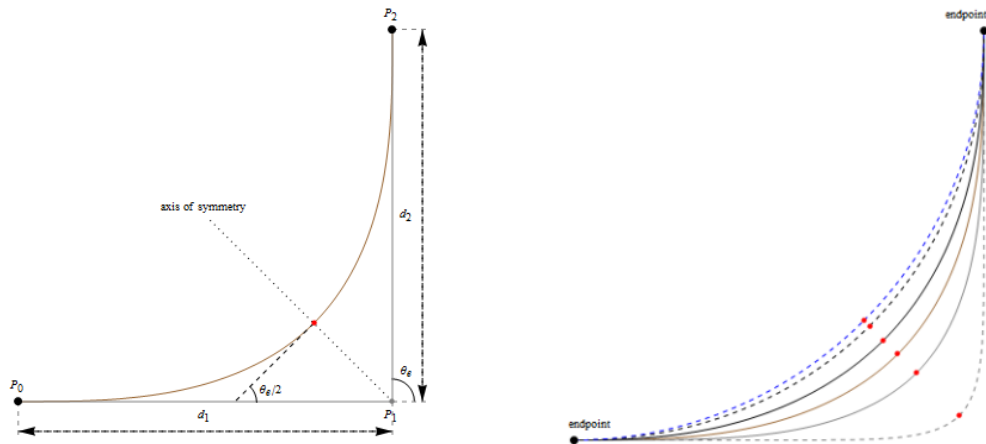


**Figure 12:** An example of symmetric C-shaped segment with  $n = 2$ . The red points indicate the joint point of a pair of spirals. Configuration represents: (a) Geometric setup, and (b) Spiral paths with various  $\alpha$  values.

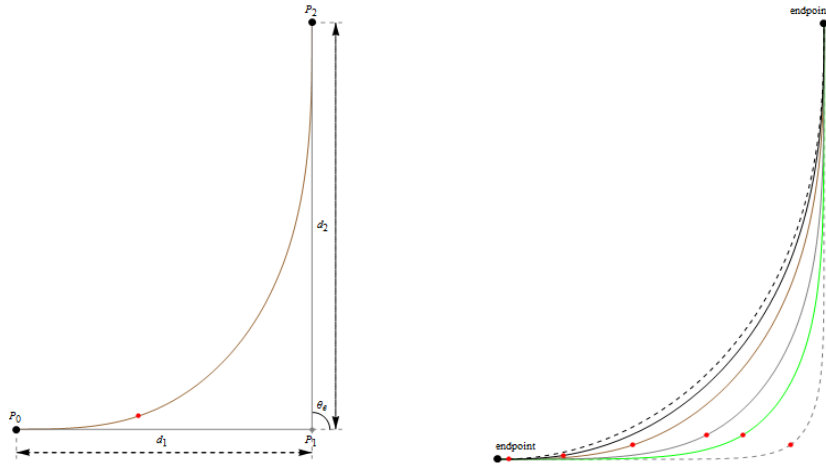


**Figure 13:** An example of asymmetric C-shaped segments with  $n = 2$ . The red points indicate the joint point of a pair of spirals. Configuration represents: (a) Geometric setup, and (b) Spiral paths with various  $\alpha$  values.

#### 4.1.3 Initializing a smooth path with default $\alpha$

We construct a smooth reference path with a default  $\alpha$  value. If users desire to obtain a smooth path which minimizes curvature variation energy  $V$ , the default  $\alpha$  is set to be  $\alpha = -1$ . Otherwise, it is set as  $\alpha = -5$ . There are three conditions we may encounter:

##### a) No solution

The solution of clothoid may not always exist. In case there is no solution, polyline path is either further partitioned into two parts or we modify the  $\alpha$  value with user defined step size  $h$ . Note that for section with  $n = 2$ , straight line can be added to the longer leg of polyline so that asymmetric case is transformed to become symmetric case. Further partition method is carried out based on the number of the line segments  $n$  of the treated section and  $n > 2$  must be hold. If  $n$  is odd, a new point is added to the midpoint of the middle line segment. Otherwise, it will be added to the midpoint of the middle line segment that is longer. Figure 14 shows an example of further partition a C-shaped section into two parts.

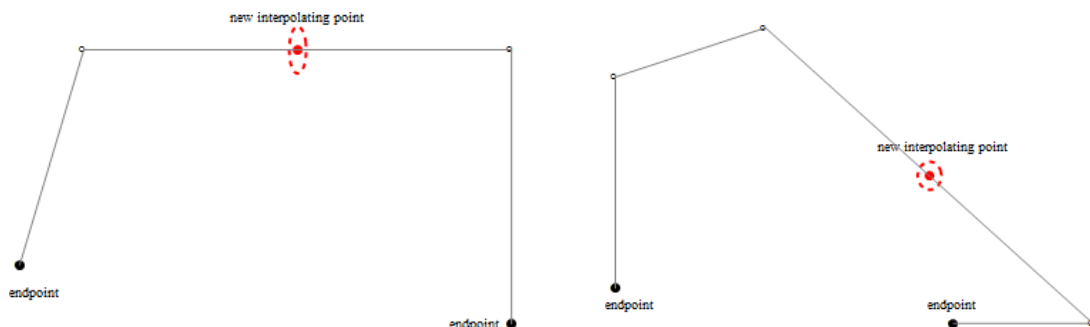


**Figure 14:** An example of further partition a C-shaped section into two parts in two conditions: (a) When  $n$  is odd, and (b) When  $n$  is even.

- b) Solution with obstacle avoidance  
 Based on the numerical results in Table 1 and Table 2, it is noticeable that  $\alpha = -1$  gives path with minimal curvature variation energy  $V$ . Therefore, in the case of minimizing  $V$ , the optimal  $\alpha$  path with its value is obtained straightaway and we end the process. For the other two cases of minimizing  $L$  and  $E$ , two additional spiral solutions are required for comparison. Without loss of generality, we modify  $\alpha$  with recommended step size  $h = 0.1$  and iteratively carrying out this process in the direction of minimizing  $M^*$ . The  $\alpha$  value will be updated iteratively until  $\nabla M^* < Tol$ . If the updated  $\alpha$  ( $\alpha_{new}$ ) has no solution, we reduce the step size  $h$  by  $h/2$  and repeat the iterative process.
- c) Solution with obstacle collision  
 We modify  $\alpha$  value with recommended step size  $h = 0.1$  iteratively until  $\nabla sp > \varepsilon$ . There are two approaches to detect collision which are based on distance threshold and point region intersection. Once we obtain a feasible spiral solution, we required another solution  $\alpha_{new}$  for comparison.  $M^*$  value of each spiral solution is calculated and compare with one another. If  $\alpha_{int}$  has minimum  $M^*$ , then it is the optimal path. Otherwise, we modify  $\alpha$  iteratively until stopping criteria is met.

**Collision Detection Algorithm based on Distance Threshold**

**Remark:** Endpoints, obstacle vertices, initial spiral path, new spiral path.

**Input :**  $P_0, P_n, v_1, \dots, v_n, \alpha, \alpha_{new}$ .

**Output:** Feasible or infeasible smooth path.

**Begin**

- Step 1 Determine intersection points  $W_1, W_2$  and represent line that joins them in standard form  $Ax + By + C = 0$ .
- Step 2 Calculate distance threshold  $\varepsilon$  as illustrated in Figure 15 by using formula  $\frac{|Ax+By+C|}{\sqrt{A^2+B^2}}$ .
- Step 3 Calculate distance of all points on the spiral path from  $\overline{P_0}, \overline{P_n}$  and identify  $sp$  (maximum distance) of  $\alpha$  path.
- Step 4 Identify  $sp_{new}$  of  $\alpha_{new}$  path.
- Step 5 Check:
  - If  $|sp_{new} - sp| > \varepsilon$
  - |  $\alpha_{new}$  path is feasible
  - else
  - |  $\alpha_{new}$  path is infeasible

**End**

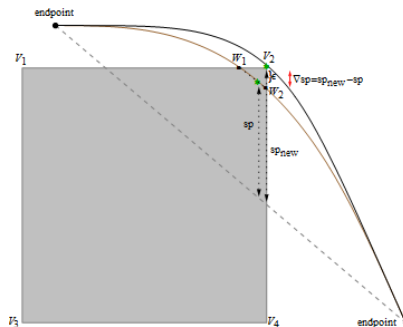


**Figure 15:** Collision detection method based on distance threshold  $\varepsilon$ .

### Collision Detection Algorithm based on Point-Region Intersection

**Remark:** Endpoints, obstacle vertices, initial spiral path, new spiral path.

**Input :**  $P_0, P_n, v_1, \dots, v_n, \alpha, \alpha_{new}$ .

**Output:** Feasible or infeasible smooth path.

#### Begin

Step 1 Identify min and max of the x and y-coordinate of obstacle (infeasible region) as shown in Figure 16.

Step 2 Calculate all points  $x_i, y_i$  along the  $\alpha$  path, where  $i = 1, \dots, n$ .

Step 3 Check:

If  $x_i, y_i \in IR$

├  $\alpha$  path is infeasible

else

└  $\alpha$  path is feasible

Step 4 Repeat Step 2 – Step 3 for  $\alpha_{new}$  path.

#### End

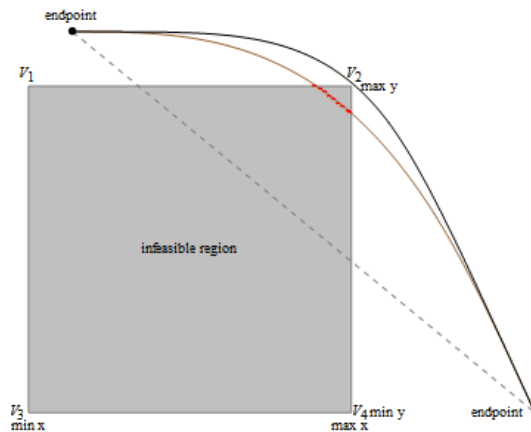


**Figure 16:** Collision detection method based on point-region intersection.

## 5 NUMERICAL EXAMPLES

This section presents few numerical examples implementing the proposed path smoothing algorithm. The implementation was performed using Wolfram Mathematica Version 9.0 on a 2.4 GHz Core i5-450M with 2 GB RAM and GeForce 310M. Figure 17 and Table 3 demonstrates the comparison between the proposed algorithm and two conventional methods used for path smoothing using cubic Bézier [9] and clothoid [15]. As shown in Figure 17, the initial Bézier and clothoid path are obviously infeasible, and thus a suitable parameter value is needed to be searched. Due to the curvature complexity of Bézier curve, its path energy is significantly greater than the clothoid and LACs path. It is easy for a clothoid path to avoid obstacle by appending straight line at both ends of the polyline path or adopt piecewise-clothoid curve as proposed in [6]. However this increases the path length. The proposed method generates a satisfactory LACs path



with minimal path length or energy, though its computation time is slightly higher than the other two methods due to the shoulder point detection process. Most of the conventional techniques of path smoothing focus on generating a collision free path alone, whereas the proposed algorithm aims to generate a collision free path with optimized path length or energy with a low computational cost. Table 3 demonstrates the computation time of each feasible path presented in Figure 17.

Figure 18 shows the result of smoothing a polyline path with clothoid using the same data points shown by Meek and Walton [15]. The numerical result of this example is demonstrated in Table 4. It is evident that LACs produce shorter path as compared to clothoid. Example 3 shown in Figure 19 consists of polyline path partitioned into four C-shaped sections whereas Example 4 has five C-shaped sections, as depicted in Figure 20. Note that the spiral paths are generated using bi-LACs with various  $\alpha$  values for each section with a desirable optimal path. The numerical results of Figure 19 and Figure 20 are demonstrated in Table 5 and Table 6, respectively. The examples clearly indicate that clothoid may fail to satisfy given polyline path where it collides with given obstacles. Furthermore, the solution of clothoid is rather limited or restricted.

With bi-LACs, user has the option to choose their desired metric to smooth the given polyline path. The experimental results show that an obstacle-avoiding smooth path with minimal path length and bending energy can be obtained when  $\alpha \rightarrow -\infty$ . Moreover, we found that  $\alpha = -1$  is the optimal spiral to produce smooth path with minimal curvature variation energy. However, it does not guarantee obstacle avoidance. Thus, user may vary the paths by either appending straight line at the polyline path or fine-tuning  $\alpha$  values to obtain other feasible obstacle-avoiding path with minimal curvature variation energy. The user insist on using clothoid, hence one may adopt piecewise-clothoid curve as proposed in [6].

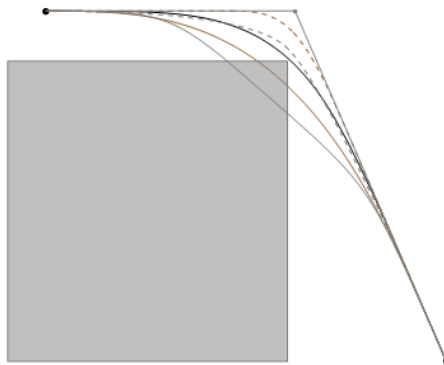


**Figure 17:** Comparison between cubic Bézier path (dashed gray), clothoid path (dashed brown) and optimal LACs path (solid black) with  $\alpha = -0.4$  using minimal path length as the metric.

Curve	Average Computation Time [s]		Metrics		
	Obstacle Avoidance	Parameters Calculation	L	E	V
Bézier	0.2	1.53	3.31	0.255	30.96
Clothoid	0.11	2	3.324	0.383	4.60
LACs	0.3	2	3.30	0.175	7.28

**Table 3:** Numerical results of Figure 17 and computation time of each path.

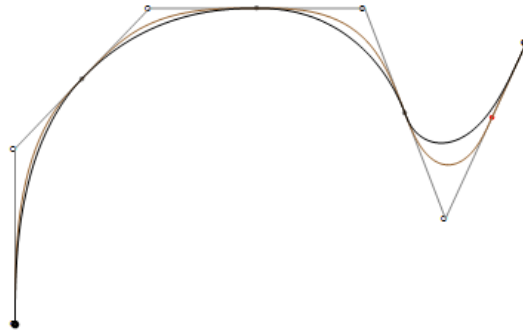


**Figure 18:** Example 2 of an optimal LACs path with minimal path length. Clothoid path is presented for comparison.

Curve (Colour)	$\alpha$				Metrics		
	Seg 1	Seg 2	Seg 3	Seg 4	L	E	V
LACs (Black)	-1.6	-3.8	-4.7	-0.7	6.8499	6.0862	1.61 $\times 10^6$
Clothoid (Brown)	-1	-1	-1	-1	7.1395	7.2703	94.684

**Table 4:** Numerical results of Figure 18.

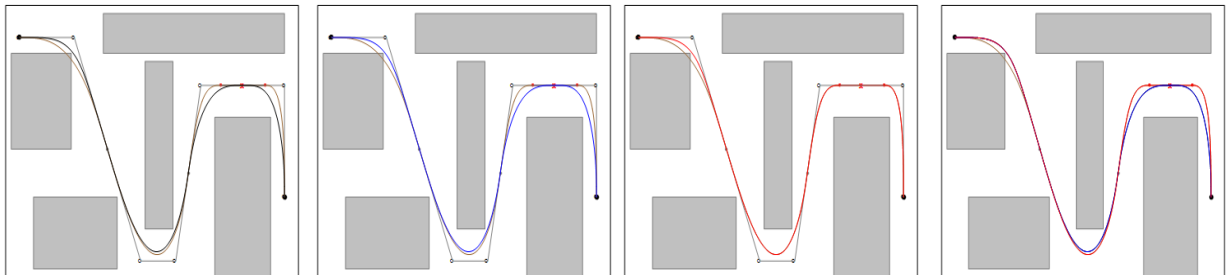


**Figure 19:** Example 3 of an optimal LAC paths with minimal path: (a) length  $L$ , (b) bending energy  $E$ , (c) curvature variation energy  $V$ , and (d) multiple paths.

Fig	$\alpha$				Metrics		
	Seg 1	Seg 2	Seg 3	Seg 4	L	E	V
19(a)	-0.4034	-1.106	-0.8	-0.6	10.4399	3.7069	14159.79
19(b)	-0.4034	-1.106	-0.8	-0.6	10.4399	3.7069	14159.79
19(c)	-0.4034	-1	-1	-1	10.6197	4.5796	122.28

**Table 5:** Numerical results of Figure 19.

## 6 CONCLUSION AND FUTURE WORK

An alternative yet simple algorithm is proposed to show the flexibility of LACs in smoothing the given polyline path with three types of metrics minimization. Furthermore, two collision detection algorithms also presented to improve the efficiency of finding the feasible smooth path. Future works include investigating path smoothing problem in uncertain environment by taking into

account additional constraints such as minimum or maximum curvature constraint and turning angle limitation. We may extend the current algorithm to yield LAC spline with  $G^3$  continuity in which designer could edit the curvature profile of LACs directly by simply inserting extra control points or by expanding the obstacle boundaries and adding knot at the obstacle point.

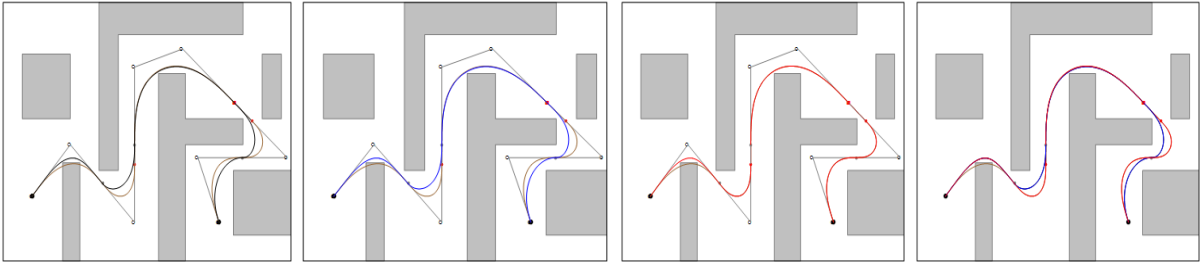


**Figure 20:** Example 4 of an optimal LAC paths with minimal path: (a) length  $L$ , (b) bending energy  $E$ , (c) curvature variation energy  $V$ , and (d) multiple paths.

Fig	$\alpha$					Metrics		
	Seg 1	Seg 2	Seg 3	Seg 4	Seg 5	L	E	V
20(a)	-0.4111	-1.5	-1.0355	-0.8	-3.826	42.6281	4.1962	198371.5
20(b)	-0.4111	-1.5	-1.0355	-0.8	-3.826	42.6281	4.1962	198371.5
20(c)	-0.4111	-1	-1	-1	-1	45.7398	4.6792	71.04

**Table 6:** Numerical results of Figure 20.

## 7 CONCLUSION AND FUTURE WORK

An alternative yet simple algorithm is proposed to show the flexibility of LACs in smoothing the given polyline path with three types of metrics minimization. Furthermore, two collision detection algorithms also presented to improve the efficiency of finding the feasible smooth path. Future works include investigating path smoothing problem in uncertain environment by taking into account additional constraints such as minimum or maximum curvature constraint and turning angle limitation. We may extend the current algorithm to yield LAC spline with  $G^3$  continuity in which designer could edit the curvature profile of LACs directly by simply inserting extra control points or by expanding the obstacle boundaries and adding knot at the obstacle point.

## 8 ACKNOWLEDGEMENTS

The authors acknowledge University Malaysia Terengganu, Ministry of Higher Education Malaysia (FRGS: 59431) and Shizuoka University for providing facilities and financial aids to carry out this research. Special thanks to anonymous reviewers for their constructive comments which improved the readability of this paper.

R. U. Gobithaasan, <http://orcid.org/0000-0003-3077-8772>

S. W. Yip, <http://orcid.org/0000-0002-8939-1882>

Kenjiro T. Miura, <http://orcid.org/0000-0001-9326-3130>

S. Madhavan, <http://orcid.org/0000-0001-7756-6086>

## REFERENCES

- [1] Anderson, E. P.; Beard, R. W.; Mclain, T. W.: Real-time dynamic trajectory smoothing for unmanned air vehicles, *IEEE Transactions on Control Systems Technology*, 13(3), 471-477. <https://doi.org/10.1109/TCST.2004.839555>
- [2] Baass, K. G.: Use of clothoid templates in highway design, *Transportation Forum*, 1(3), 1984, 47-52.
- [3] Gobithaasan, R. U.; Teh, Y. M.; Piah, A. R. M.; Miura, K. T.: Generation of Log-aesthetic curves using adaptive Runge-Kutta methods, *Applied Mathematics and Computation*, 246, 2014, 257-262. <https://doi.org/10.1016/j.amc.2014.08.032>
- [4] Gobithaasan, R. U.; Yip, S. W.; Miura, K. T.: Log-aesthetic curves for shape completion problem, *Journal of Applied Mathematics*, 2014, Article ID 960302, 10 pages. <https://doi.org/10.1155/2014/960302>
- [5] Gobithaasan, R. U.; Miura, K. T.: Logarithmic curvature graph as a shape interrogation tool. *Applied Mathematical Sciences*, 8(16), 2014, 755-765. <https://doi.org/10.12988/ams.2014.312709>
- [6] Havemann S., Edelsbrunner, J., Wagner, P., Fellner, W.D: Curvature-controlled curve editing using piecewise clothoid curves. *Computers & Graphics*, 37(6): 764-773 (2013) <https://doi.org/10.1016/j.cag.2013.05.017>
- [7] Hickerson, T. F.: *Route Location and Design*, McGraw-Hill, New York, 1964.
- [8] Levien, R.; Séquin, C.: Interpolating splines: which is the fairest of them all?, *Computer-Aided Design and Applications*, 6(1), 2009, 91-102. <https://doi.org/10.3722/cadaps.2009.91-102>
- [9] Li, Z.; Meek, D.; Walton, D.: A smooth, obstacle-avoiding curve, *Computers and Graphics*, 30(4), 2006, 581-587. <https://doi.org/10.1016/j.cag.2006.03.003>
- [10] Miura, K. T.: A general equation of aesthetic curves and its self-affinity, *Computer-Aided Design and Applications*, 3(1-4), 2006, 457-464. <https://doi.org/10.1080/16864360.2006.10738484>
- [11] Miura, K. T.; Sone, J.; Yamashita, A.; Kaneko, T.: Derivation of a general formula of aesthetic curves, In *Proceedings of the 8<sup>th</sup> International Conference on Humans and Computers (HC2005)*, University of Aizu, 2005, 166-171.
- [12] Miura, K. T.; Shibuya, D.; Gobithaasan, R. U.; Usuki, S.: Designing log-aesthetic splines with  $G^2$  continuity, *Computer-Aided Design and Applications*, 10(6), 2013, 1021-1032. <https://doi.org/10.3722/cadaps.2013.1021-1032>
- [13] Suzuki, T.: Application of log-aesthetic curves to the eaves of a wooden house, 4<sup>th</sup> International Conference on Archi-cultural Interactions through the Silk Road, Mukogawa Women's University, Nishinomiya, Japan, July 16-18, 2016.
- [14] Walton, D. J.; Meek, D. S.: A planar cubic Bézier spiral, *Journal of Computational and Applied Mathematics*, 72(1), 1996, 85-100. [https://doi.org/10.1016/0377-0427\(95\)00246-4](https://doi.org/10.1016/0377-0427(95)00246-4)
- [15] Walton, D. J.; Meek, D. S.: A controlled clothoid spline, *Computers and Graphics*, 29, 2005, 353-363. <https://doi.org/10.1016/j.cag.2005.03.008>
- [16] Yoshida, N.; Saito, T.: Interactive aesthetic curve segments, *The Visual Computer*, 22(9-11), 2006, 896-905. <https://doi.org/10.1007/s00371-006-0076-5>